NRL Report 7968

Modulation of Microwave Backscatter by Gravity Waves in a Wave Tank

W. C. KELLER AND J. W. WRIGHT

Physical Oceanography Branch
Ocean Sciences Division

March 29, 1976

NAVAL RESEARCH LABORATORY
Washington, D.C.

REPORT DOCUMENTATION PAGE

READ INSTRUCTIONS BEFORE COMPLETING FORM

1. REPORT NUMBER: NRL Report 7968
2. GOVT ACCESSION NO.:
3. RECIPIENT'S CATALOG NUMBER:

4. TITLE (and Subtitle): MODULATION OF MICROWAVE BACKSCATTER BY GRAVITY WAVES IN A WAVE TANK

5. TYPE OF REPORT & PERIOD COVERED: Interim report on a continuing NRL Problem

6. PERFORMING ORG. REPORT NUMBER:

7. AUTHOR(s): W.C. Keller and J.W. Wright

8. CONTRACT OR GRANT NUMBER(s):

9. PERFORMING ORGANIZATION NAME AND ADDRESS: Naval Research Laboratory, Washington, D.C. 20375

10. PROGRAM ELEMENT, PROJECT, TASK AREA & WORK UNIT NUMBERS: NRL Problem G01-14.101, Project RR 031-03-41

11. CONTROLLING OFFICE NAME AND ADDRESS: Office of Naval Research, Arlington, Va. 22217

12. REPORT DATE: March 29, 1976

13. NUMBER OF PAGES: 24

14. MONITORING AGENCY NAME & ADDRESS (if different from Controlling Office):

15. SECURITY CLASS. (of this report): Unclassified

15a. DECLASSIFICATION/DOWNGRADING SCHEDULE:

16. DISTRIBUTION STATEMENT (of this Report): Approved for public release; distribution unlimited.

17. DISTRIBUTION STATEMENT (of the abstract entered in Block 20, if different from Report):

18. SUPPLEMENTARY NOTES:

19. KEY WORDS (Continue on reverse side if necessary and identify by block number):
Doppler spectra
Imaging radar
Microwave scatter
Ocean waves
Sea clutter

20. ABSTRACT (Continue on reverse side if necessary and identify by block number):

Modulation of coherent microwave backscatter at 9.375 GHz, vertical polarization, and at a depression angle of 45° has been measured in a wind wave tank as a function of windspeed, modulating wave frequency, and amplitude. A relaxation time model can be used to describe the phase and magnitude of the modulation for windspeeds of less than about 7 to 8 m/s and wave slopes of less than about 0.1; the magnitude of the modulation depends strongly on windspeed and direction. Marked deviations from the model occur at the highest wind utilized (10 m/s), and the small-scale wind-generated waves coalesce near or behind the crests of the modulating

(Continued)

20. ABSTRACT (Continued)

lating wave. The orbital velocity of the large waves is deduced to an accuracy of 3 cm/s or 10% from the measurements of modulated doppler shift, though the phase of the modulated doppler shift exhibits windspeed dependence apparently due to the wind drift. Mean scattering cross sections show a substantial dependence on modulating wave amplitude for intermediate windspeeds. The implication of the measurements for radar imaging of ocean waves is discussed. It is concluded that the modulation of line-of-sight scatterer speed is a much more reliable measure of ocean wave amplitude than the amplitude modulation of backscattered power.

CONTENTS

MODULATION OF MICROWAVE BACKSCATTER BY GRAVITY WAVES IN A WAVE TANK

INTRODUCTION

One of the universal features of wind-generated wave systems is the modulation of velocity and amplitude of small scale waves by longer and larger waves. These modulations are of practical importance. For example, microwave radars intended for remote sensing of ocean waves depend on the modulation of surface scatterer density or velocity for their imaging properties. Furthermore, the short gravity and capillary waves, which are the predominant microwave scatterers under many oceanic conditions, can support the entire stress of the wind on the water [1]. If the larger waves modulate the small wave amplitude, they also modulate this stress. The component of this modulated stress which is in phase with the horizontal component of orbital speed of the large wave will work on the large wave and cause it to grow. The mechanism of energy transfer between short and long waves discussed by Hasselmann [2] also depends on the phase and amplitude of this modulation. Results were recently reported [3] of some laboratory microwave scattering experiments designed to test a phenomenological theory of this modulation. This theory, which is designated the relaxation time model, was successful over a certain range of windspeeds and modulating wave frequencies and amplitudes. This report is concerned with the observed departures from the model and with measurements from the same experiments of modulated surface speeds using the doppler effect.

EXPERIMENTAL TECHNIQUES AND FACILITIES

These results were obtained from the same series of experiments which were reported previously [3]. The experimental facilities, methods, data processing, and notation used in this report are the same as in the earlier one. All measurements were made with focused parabolic antennas [4], on vertical polarization, at 9.375 GHz, and at a depression angle of 45°. Both upwind and downwind looks were used, as shown in Fig. 1. Homodyne microwave detection with a 400-Hz IF was used. Power spectra of this homodyne-detected signal are called doppler spectra. Those shown in Figs. 2 and 3 illustrate one of the experimental problems encountered in indoor scattering measurements-room reflections. Of course, reflections which are not doppler shifted are simply nulled with a microwave bridge. The troublesome reflections in this case are those which are essentially specularly reflected from the wave and rescattered back to the antenna from stationary objects in the room. Because the large wave slopes are not greater than 0.3 rad, the specular planes are nearly horizontal; it is largely the vertical component of large-wave orbital speed which shifts the frequency of these near-specular reflections. Because the vertical motions must have a zero mean value, reflections from this source tend to produce peaks

Manuscript submitted December 22, 1975.

placed nearly symmetrically about the origin as in the cases $u_* = 0$ in Figs. 2 and 3. The wind-generated backscatter, on the other hand, is the result of small wind-generated waves traveling at their own speed. The doppler spectra from this source are thus shifted in the direction of the wind. As the wind increases the backscatter increases, but the specular scatter may actually decrease due to the roughening of the large wave surface. Thus the room reflections, as revealed by the peak marked "S" on the upwind side of the spectra in Figs. 2 and 3, are more significant at lower winds and larger modulating wave amplitudes. In these cases it was usually possible to use the microwave absorbing screen (Fig. 1) to control them satisfactorily.

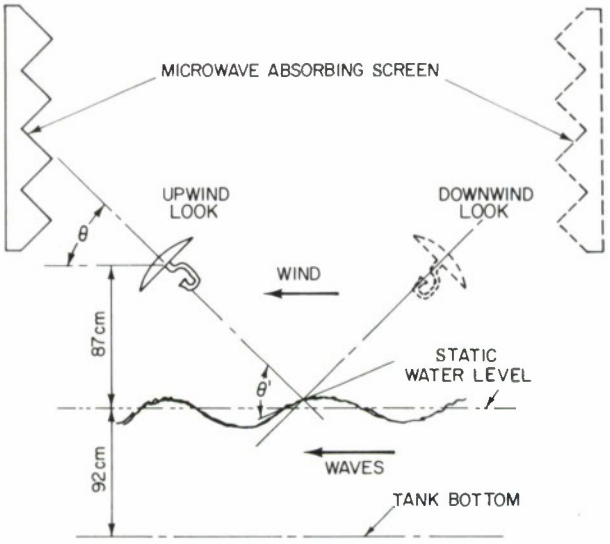

Fig. 1 — Schematic of the scattering experiment

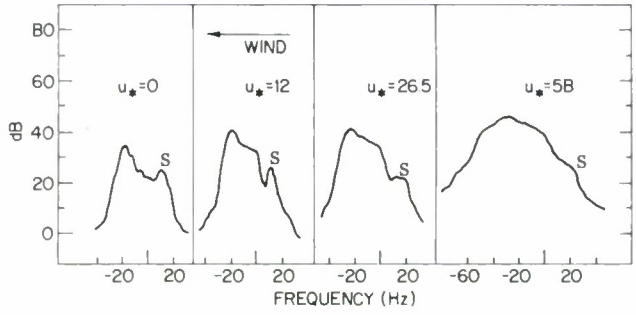

Fig. 2 — Doppler spectra looking upwind. The modulating wave frequency was 1.1 Hz, and $U_0/C = 0.15$.

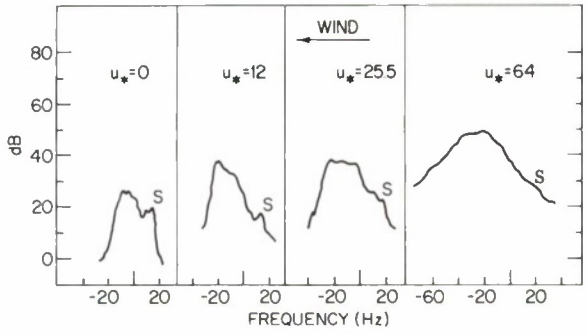

Fig. 3 — Doppler spectra looking downwind. The modulating wave frequency was 0.575 Hz, and U_0/C = 0.09.

A second problem is that of contaminant films on the water surface. Previously we found [1] that these could be eliminated by blowing for a sufficient length of time while draining the tank slowly and continuously through a standpipe at the beach end. Measurements of mean-scattering cross section taken in conjunction with the data reported here are compared (Fig. 4) with similar measurements at 30° [5] in the NRL wavetank where it is known [1] that surface films are removed. The values are 4 to 6 dB higher than those measured in the NRL tank, as expected from the higher depression angle. The rapid rise occurring at the same low windspeed in both tanks is a further indication of absence of surface films. On a few occasions it was noted that the cross sections were lower than those in Fig. 4 and increased slowly with time during the initial period after turning on the wind. This was judged the result of surface active material slowly being removed by the action of the wind. Consequently, the wind was allowed to blow at least 30 min before measurements were made.

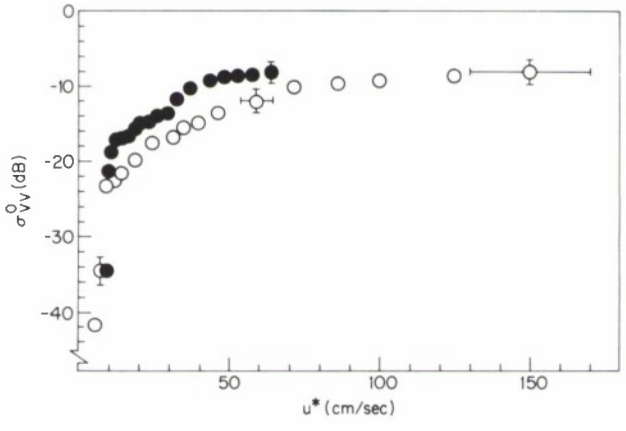

Fig. 4 — Scattering cross section looking upwind as a function of air friction velocity: ○ 12-m fetch, 30° VV, NRL tank; ● 7-m fetch, 45° VV, University of Florida tank.

Finally, the fetches given here are those measured from the end of the entrance air channel which was elevated above the mean water level to allow the passage of the plunger-generated waves. Furthermore, several roof sections were removed from the tank. Thus the numbers given for fetch are, to a degree, nominal, and the peak frequencies of the wind-generated waves given in connection with Figs. 5, 6, and 7 should be used in comparing the wind-generated waves with those in other tanks.

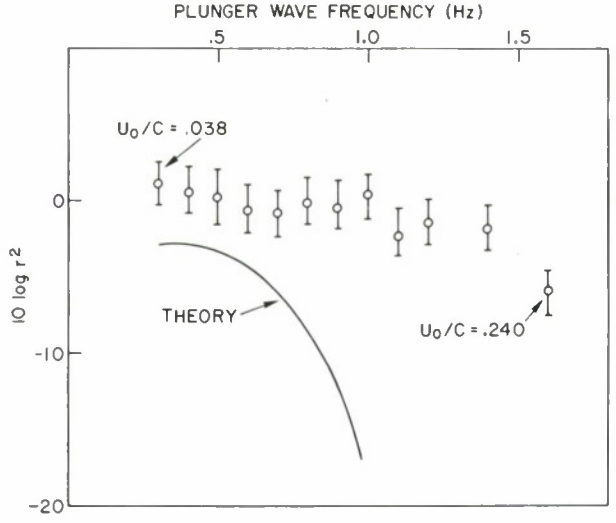

Fig. 5 — Measured and calculated diminution of wind-generated waves by plunger-generated waves: $u_* = 64$ cm/s, plunger-wave amplitude ≈ 2.9 cm, peak-wind wave frequency = 3.2 Hz, phase speed of dominant wind wave = 49 cm/s, $q_0 = 35$ cm/s.

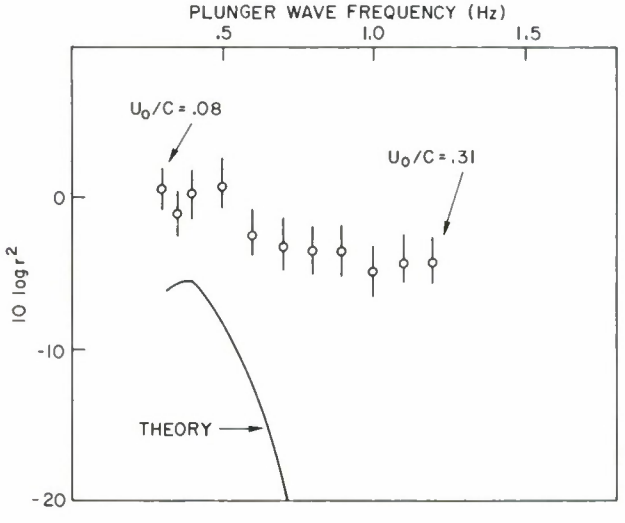

Fig. 6 — Measured and calculated diminution of wind waves: plunger-wave amplitude ≈ 6 cm; other parameters as in Fig. 5.

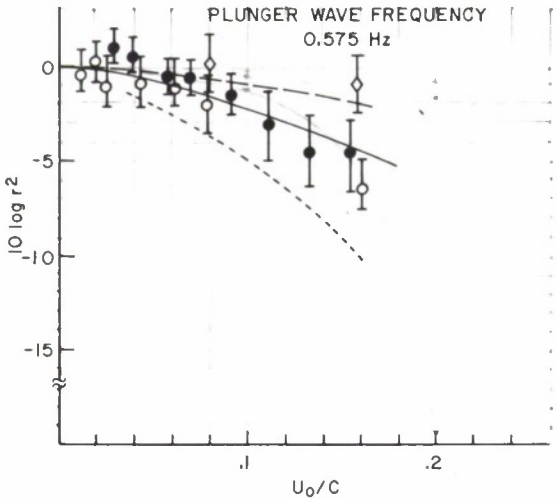

Fig. 7 — Measured and calculated diminution of wind waves by 0.575-Hz plunger-generated waves.

u_*	Measured r^2	Theor. r^2	Peak frequency of wind waves
16.5	◇	– – – –	4.2 Hz
30	◆	———	3.4 Hz
64	◇	- - - - - -	3.0 Hz

THE AUGMENTED WIND DRIFT

When the wind blows across the water, a highly sheared current develops near the surface extending a few millimeters into the water. The surface speed of this current, or wind drift as it is often called, amounts to 3 to 4% of the wind speed. The influence of the wind drift on the phase speed of wind-generated short gravity and capillary waves is clear [6-8]. Now, Banner and Phillips [9] have pointed out that the wind drift may also act to limit the amplitude of short waves. The idea is that the wind drift is sufficiently augmented by interaction with the orbital velocity field of the wave that the maximum particle speed may exceed the phase speed, and the wave breaks.

Banner and Phillips [9] calculated the modifications produced in the wind drift by an underlying irrotational wave. They neglect the effect of the wind on the linear dynamics of the wave (e.g., the change in phase speed) but find that the surface drift is augmented in the mean as well as by an oscillating component. The total augmented surface drift q is given by

$$q = (C_o - U) - [(C - U) - q_o\ (2C - q_o)]^{1/2}, \tag{1}$$

where

U is the tangential component of orbital velocity just under the wind drift

C is the phase speed of the irrotational wave

q_o is, for practical purposes, the surface drift in the absence of the wave.

The total horizontal particle velocity is then, very nearly, $q + U$. If $q_o/C \equiv X$ is not too large, it is perspicuous to expand Eq. (1) in a Taylor series in U/C to second order;

$$q + U = q_o + \frac{U}{1 - x} + \frac{x\,(1 - x/2)}{(1 - x)3}\,\frac{U^2}{C} + \ldots. \tag{2}$$

The linear term on the right of Eq. (2) is the horizontal component of surface speed obtained from a first-order perturbation of the wind drift [8]. This form will be useful in discussing the doppler measurements of surface speed given in the section, "Microwave Measurement of Orbital Speeds."

If the total horizontal particle velocity $q + U$ exceeds C, the wave breaks. Phillips and Banner [10] suppose that short gravity waves in wind wave tanks are limited, or brought to a steady state, by this form of breaking. Then, if an underlying larger and longer wave is applied, the wind drift is further augmented, causing premature breaking of the short gravity waves. Phillips and Banner [10] estimate that the ratio ρ of wind-wave amplitude in the presence of a longer wave to the undiminished amplitude is

$$\rho = (g/g')\left(\frac{C_c - q_{\max}}{C - q_o}\right)^2, \tag{3}$$

where

g is the acceleration of gravity

g' is the effective acceleration of gravity at the large wave crest

C_c is the phase speed of the short wave at the large wave crest

$q_{\max}$ is the maximum value of the augumented wind drift.

We measured wind-wave spectra as a function of large-wave amplitude and frequency using the capacitance wave probe and obtained the mean-squared surface displacement of the wind waves by numerical integration of these spectra. The ratio of this mean-squared displacement in the presence of mechanically generated waves to that in the absence of these waves is plotted in Figs. 5, 6 and 7. In the case of the data of Figs. 5 and 6, the windspeed was 10 m/s ($u_* = 64$ cm/s), the fetch was 6.0 m, and the wave amplitude was nearly constant at 2.9 cm and 6.0 cm, respectively; the wave frequency was varied. The value of ρ^2 calculated from Eq. (3) is the solid curve in both cases. It is evident that the predicted diminution is much too great. In the data of Fig. 7, the wave frequency was kept constant at 0.575 Hz and the amplitude varied at two lower windspeeds ($u_* = 16.5$ and 30 cm/s), but there was a somewhat longer fetch, about 8.0 m. The solid and dotted lines are again the predictions calculated from (3). The predicted values at the lower windspeed are now too small, although at $u_* = 30$ cm/s the predicted and observed values are very close. It should be noted that this is the same windspeed at which Phillips and Banner [10] obtained a reasonable agreement between theory and experiment. Although there is a scarcity of data at low windspeeds, it does appear that the windspeed dependence of the measured diminishment of wind-wave amplitude is the opposite of that predicted.

MODULATION OF SCATTERING CROSS SECTION

Modulation measurements are reported in terms of a quantity M called the fractional modulation. This quantity is defined in terms of the measured autocovariance $R(\tau)$ of the

linearly (i.e., homodyne) detected and rectified microwave signal $e(t)$ which has random and periodic components $f(t)$ and $u(t)$, respectively:

$$e(t) = f(t) + (r)^{1/2}\, u(t). \tag{4}$$

Then

$$M \equiv r/R(0). \tag{5}$$

This quantity is defined [3] in such a way that if the variation in backscattered power, or local scattering cross section, is proportional to U_0/C (U_0 being the horizontal component of orbital speed and C being the phase speed of the large wave), then M is proportional to $(U_0/C)^2$. There is, furthermore, an empirically determined statistical factor, the ratio of the squared mean scattered field to mean squared scattered field, in the proportionality. Thus, when the local scattering cross section σ is approximately proportional to U_0/C, the ratio of maximum to minimum cross section is

$$\sigma_{max}/\sigma_{min} \approx \left[\frac{1 + 1.7\, M^{1/2}}{1 - 1.7\, M^{1/2}}\right]^2. \tag{6}$$

A value for M of 0.1 corresponds to a peak-to-peak cross-sectional ratio of nearly 10 dB. The experimental determination of r as the peak-to-peak amplitude of the periodic portion of an autocovariance effectively discriminates against modulations at the second harmonic of the large-wave frequency, so that Eq. (6) has an approximate validity even when the modulation in scattering cross section is not small. The value of M corresponding to $\sigma_{min} \to 0$ in Eq. (6) is about 0.36. It will be seen that this is close to the maximum observed value of M which occurred when portions of the large wave were visibly quite smooth.

Conventional capacitance probes made from No. 36 magnet wire were used to measure the large-wave amplitudes. The phase of modulation in backscattered power and that of the line-of-sight velocity reported in the section "Microwave Measurement of Orbital Speeds" were obtained by crosscorrelation with the output of the capacitance probe. The phase obtained by crosscorrelation of $e(t)$ with the capacitance probe output is denoted φ_C and is the phase angle by which the modulated microwave return leads the wave crest. This quantity is given (Fig. 8) as a function of windspeed for the case of modulation by a 4.20-m wave for which $U_0/C = 0.09$, and comes from the same runs as the data of Fig. 3 and Fig. 5 of Keller and Wright [3]. The solid curves of Fig. 8 were calculated from Eq. (34) of Ref. 3. Figure 8 illustrates the rapid coalescence of scatterers near the wave crest at air friction velocities exceeding 40 cm/s. This is a striking departure from the prediction of the relaxation theory shown by the solid lines. Note that the plunger wave was of moderate amplitude in this case ($U_0/C = 0.09$) and that the fractional modulation from Fig. 3 of Ref. 3 was only 0.02 to 0.04 at $u_* = 64$ cm/s. The windspeed dependence of φ_C for both upwind and downwind looks in the case of modulation by a 1.1-Hz wave with $U_0/C = 0.15$ is similar and is shown in Fig. 9. Note that the error in φ_c resulting from boresighting, etc., is a linear error so that the error in phase is much larger, perhaps 20°, at 1.1 Hz.

The fractional modulation looking both upwind and downwind for $u_* = 64$ cm/s for the case of modulation by a 0.9-Hz wave is given as a function of U_0/C in Fig. 10. These measurements were made at a shorter fetch than those of Figs. 8 and 9; the peak frequency of the wind-wave system in the absence of the 0.9-Hz wave was 3.6 ± 0.2 Hz. The phase φ_C for these cases is shown in Fig. 11. Note that the phase is relatively independent of modulating wave amplitude for $U_0/C < 0.2$ but decreases markedly thereafter.

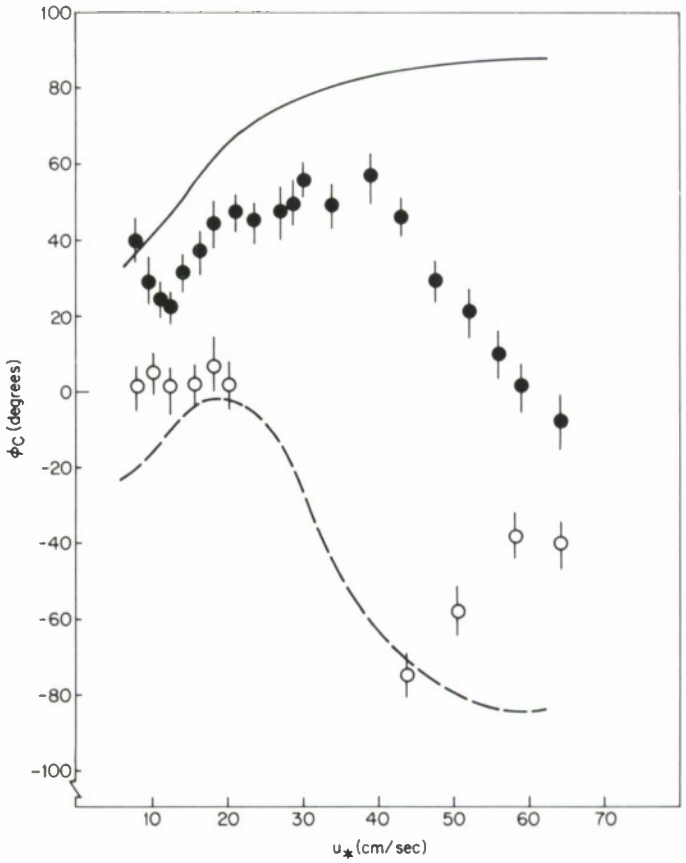

Fig. 8 — The phase by which the modulated scattered power leads the wave crest. Wave frequency = 0.575 Hz, U_0/C = 0.09, ● upwind look, ○ downwind look.

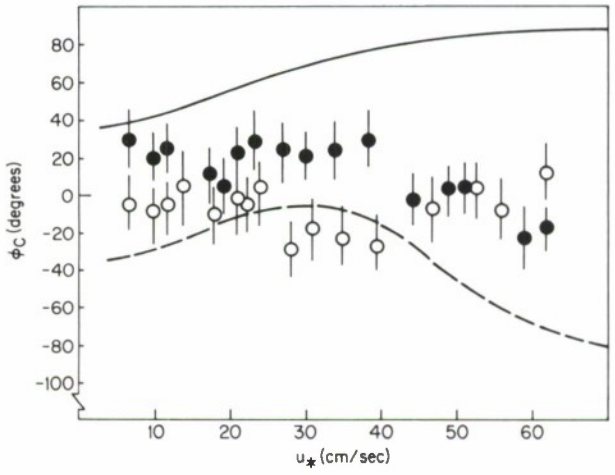

Fig. 9 — The phase by which the modulated scattered power leads the wave crest. Wave frequency = 1.1 Hz, U_0/C = 0.15, ● upwind look, ○ downwind look.

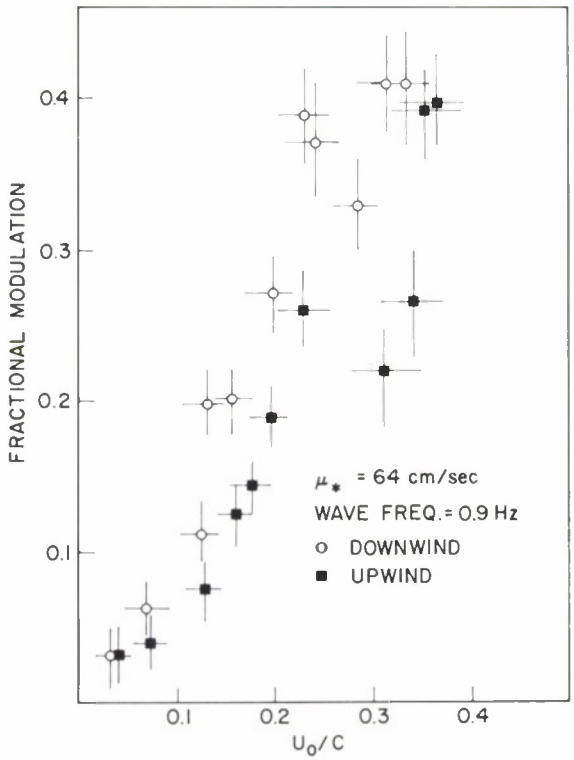

Fig. 10 — Fractional modulation as a function of wave amplitude at u_* = 64 cm/s, fetch = 4 m, and modulating wave frequency = 0.9 Hz; ♦ upwind look, ◇ downwind look.

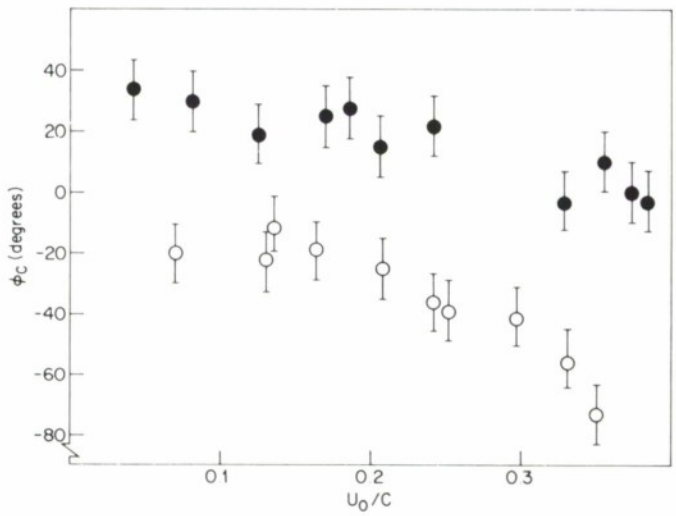

Fig. 11 — The phase by which the modulated scattered power leads the wave crest as a function of wave amplitude at u_* = 64 cm/s, fetch = 4 m, and modulating wave frequency = 0.9 Hz; ♦ upwind look, ◇ downwind look.

Finally, several runs were made in which the windspeed and modulating wave amplitude were held constant and the wave frequency was varied. The fractional modulation looking downwind at $u_* = 64$ cm/s from these runs is plotted vs U_0/C in Fig. 12, together with data from several fixed-frequency cases under the same wind conditions. One might infer from these data that the fractional modulation at $u_* = 64$ cm/s depends only on U_0/C and is independent of wave frequency. This must be a cautious inference, however, for all fractional modulations greater than 0.2 (Fig. 12) occur for wave frequencies of 0.9 Hz or greater. The phase φ_C for the variable frequency runs is plotted vs frequency in Fig. 13, but only those cases are included for which $U_0/C \leqslant 0.2$. Phases from fixed-frequency runs at the same fetch are again included and agree reasonably well with the rest. The data show that the scattering cross section looking downwind is always a maximum on the windward (back) side of the wave, but the phases exhibit a curious oscillatory dependence on the wave frequency. This behavior may be fetch dependent, however, because the phase φ_C in the case of 0.9-Hz waves with $U_0/C < 0.2$ (Fig. 11) at a shorter fetch and the same wind conditions is significantly different.

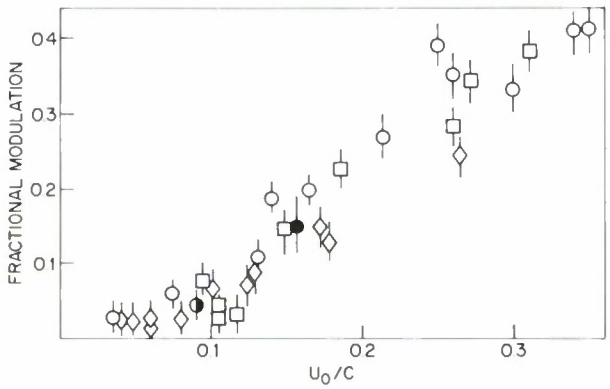

Fig. 12 — Fractional modulation as a function of U_0/C at $u_* = 64$ cm/s, 7-m fetch for various modulating wave frequencies.

◑ - 0.575 Hz, ● - 1.1 Hz, ○ - 0.9 Hz
□ - variable frequency amplitude ≈ 6.0 cm
◇ - variable frequency amplitude ≈ 2.9 cm

MICROWAVE MEASUREMENT OF ORBITAL SPEEDS

The microwave system is coherent so that it receives a signal which preserves phase variations (i.e., doppler shifts) in the audio-frequency range. These doppler shifts are offset 400 Hz to prevent folding. We measured the doppler shift by applying the homodyne-detected microwave signal to an analog frequency-to-voltage converter. This is a device which yields an output voltage proportional to the frequency of the input signal but independent of the input voltage amplitude over a relatively wide range of input levels. Some of the signals however, exhibited nearly 100% modulation as previously described. The input voltage was amplified and, of necessity, limited to lift the low-level portions of the signal over the threshold of the converter.

The limiting process tends desirably, to give a signal which, as counted by the converter, has the average frequency of the input. Multiplication by $\lambda/2\cos\theta$ converts measured doppler shifts to line-of-sight scatterer speed. Denote this line-of-sight scatterer speed by $v(t)$. The autocovariance $V(\tau)$ of $v(t)$ has a form analogous to the examples of autocovariance of the microwave signal $e(t)$ shown in Fig. 2 (left) of Keller and Wright [3]. That is, it exhibits a spike at $\tau = 0$, presumably due to the wind-generated waves, a mean or DC value due to the mean scatterer speed, and a periodic portion due to the modulating wave. The peak-to-peak amplitude of the periodic portion of $V(\tau)$ is used as the measure of modulated scatterer speeds. This procedure, as in the case of $e(t)$ and $R(\tau)$, discriminates against the second harmonic of the periodic portion of $v(t)$. Therefore the peak-to-peak amplitude of the periodic portion of $V(\tau)$ is very nearly the square of the amplitude v_0 of the fundamental component of $v(t)$. The capacitance probe records were analyzed in an entirely analogous way so that in comparing scatterer speed with line-of-sight orbital speed calculated from the wave-height records, as described later, amplitudes of components are always being compared at the fundamental modulating wave frequency.

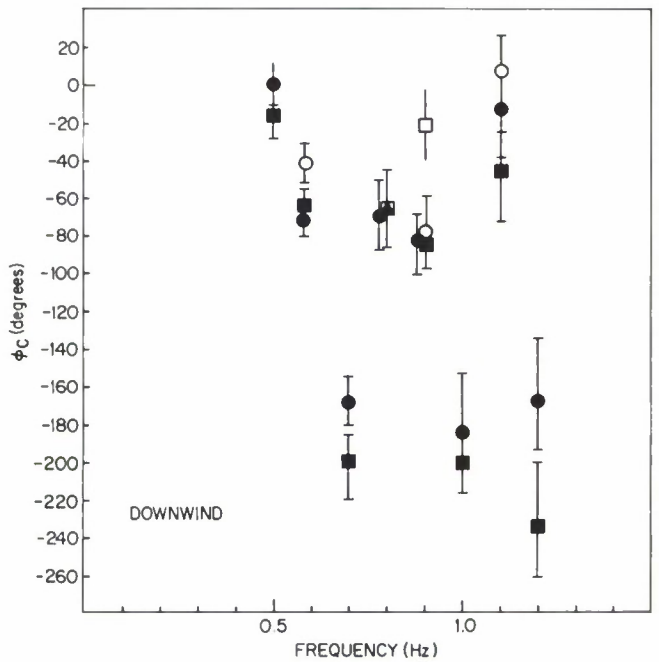

Fig. 13 — The phase by which the modulated scattered power leads the wave crest as a function of modulating wave frequency, at $u_* = 64$ cm/s.

● - variable frequency, 6.0-cm wave, 7-m fetch
■ - variable frequency, 2.9-cm wave, 7-m fetch
○ - other fixed frequency runs, 7-m fetch
□ - 0.9 Hz, 4-m fetch

It remains to relate the line-of-sight scatterer speed to the orbital speed of the large wave. Suppose, first, that the horizontal and vertical components of scatterer speed are u and w, respectively, so that the line-of-sight scatterer speed is just u cos θ + w sin θ. If u and w are equal in magnitude and separated by 90° in phase, as in the case of the circular orbits of a deep water wave, and if $u = U_0 \cos \Omega t$, then

$$V_s = U_0 \cos (\Omega t + \theta). \tag{7}$$

The line-of-sight speed then equals the orbital speed and leads the wave crest by a phase angle equal to the depression angle.

In the case of the longer plunger-generated waves in our experiments, the finite depth of the tank was significant and the first order (in U_0/C) orbits elliptical. In that case,

$$V_s = U_0 \left[\cos^2\theta + \sin^2\theta \tanh^2 Kd\right]^{1/2} \cos (\Omega t + \phi_D) \tag{8a}$$

$$\tan \phi_D = \tanh Kd \tan \theta, \tag{8b}$$

where U_0 is now the magnitude of the horizontal component of fluid motion and ϕ_D is the angle by which the line-of-sight speed leads the wave crest.

If the scatterers are Bragg scatterers, they travel at their own phase speed C_s, which includes the advective effect of the wind drift. Because the wind drift is very thin, the small waves are not advected by the full surface current. For X-band scatterers,

$$C_s = C_0 + \alpha q \tag{9}$$

was found [4] where $\alpha \approx 0.7$. There are two effects. First, the wind drift is augmented by the orbital velocity of the large wave as described in the section on wind drift. Second, the vertical velocity of the small wave is diminished below the vertical component of fluid velocity because the small waves are propagating upward where the vertical component of fluid velocity is downward and vice versa. The result is that, to first order in U_0/C and for $\theta = 45°$ and 135°,

$$V_s \cong U_0 \left[\frac{1 + \tanh^2 Kd}{2} + \frac{\alpha q_0 - C_s \tanh Kd}{C}\right]^{1/2} \cos (\Omega t + \phi_D) \tag{10}$$

and

$$\tan \phi_D = \pm \frac{(1 - q_0/C)\left(1 - \dfrac{C_0 + \alpha q_0}{C}\right) \tanh Kd}{1 + (\alpha - 1)\, q_0/C}, \tag{11}$$

where

$$U_0 = \Omega A / \tanh Kd \tag{12}$$

and A is the wave amplitude. Modulation of the thickness of the wind drift has been neglected in deriving Eqs. (10) and (11). The second term in brackets on the right of Eq. (10) leads to a difference between scatterer and orbital speeds of less than 10% in nearly all cases treated here. Because the probable error in capacitance probe calibration was of this order, we have neglected this correction in comparing doppler and capacitance probe measurements in Figs. 14 and 15. No systematic, significant difference between V_0 and the line-of-sight orbital speed calculated from the probe measurements is evident.

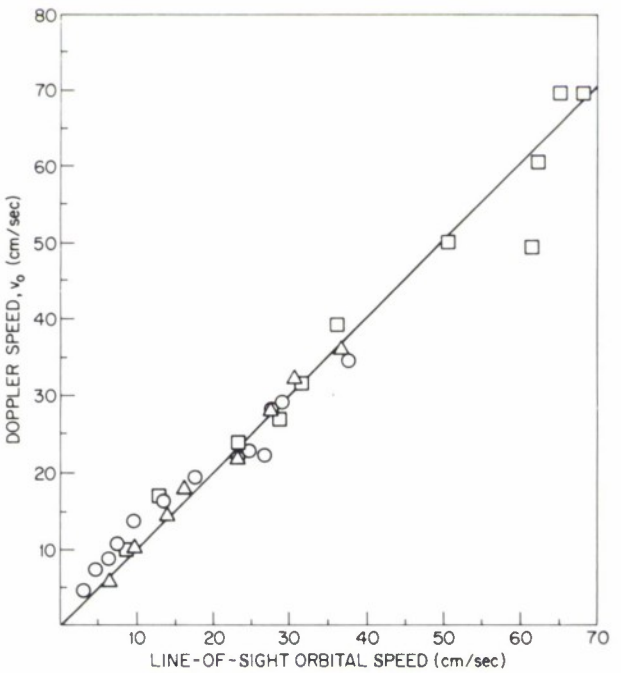

Fig. 14 — Comparison of measured line-of-sight scatterer speed (doppler speed) with line-of-sight orbital speed calculated from wave amplitude.

○ - u_* = 16.5 cm/s, 0.575 Hz
△ - u_* = 30 cm/s, 0.575 Hz
□ - u_* = 64 cm/s, 0.9 Hz

Because the vertical scatterer speed is diminished and the horizontal speed increased over the corresponding orbital speeds, one would expect the phase of the measured line-of-sight speed to be more detectably affected. This is indeed the case, as can be seen in Figs. 16 and 17 where φ_D is plotted vs u_* . The measured phases agree well with those calculated from Eq. (11) when the antenna looks upwind, but there is a significant deviation at higher winds for the downwind look. In the case of the 1.1-Hz wave, the line-of-sight speed looking downwind actually appears to lead the crest. The same behavior is apparent in the data for the 0.9-Hz wave (Fig. 18) which furthermore includes cases for which U_0/C varies from 0.10 to 0.23.

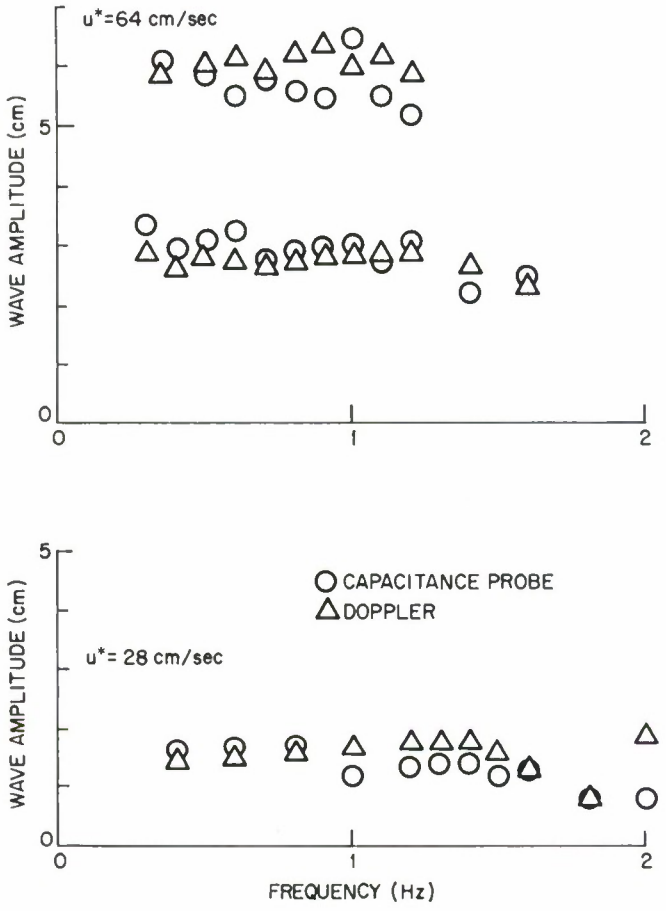

Fig. 15 — Comparison of wave amplitude calculated from doppler speed with measured wave amplitude: ○ - capacitance probe, △ - doppler.

SUMMARY OF WAVE-TANK MEASUREMENTS

In previous work a phenomenological theory was developed [3] that describes the response of wind-generated waves to straining. This theory is called the relaxation time model. This model describe the perturbation of the small-scale wind-generated wave spectrum by the horizontal component of orbital velocity of the large wave by an expansion in U_0/C. That is,

$$F(k) = F_0(k) + f_1(k)\ U_0/C + f_2(k)(U_0/C)^2 + \ldots\ , \tag{13}$$

where $F(k)$ is the surface displacement spectrum of the wind-generated wave system. (See also Ref. [1], Eq. (17).)

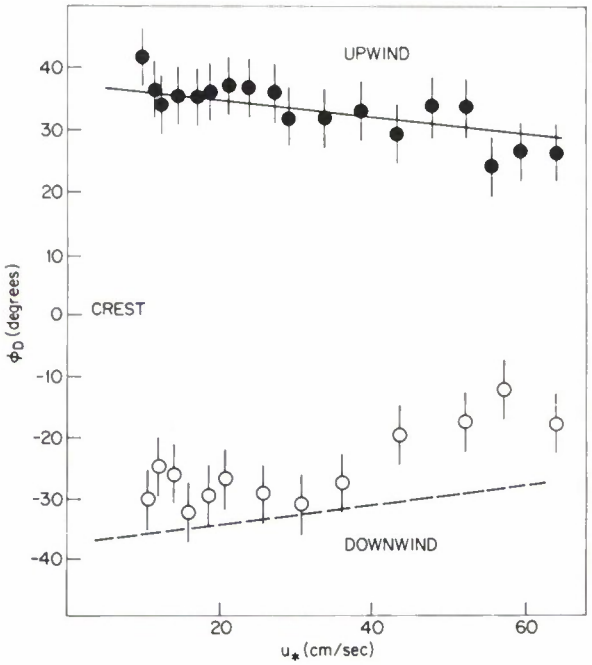

Fig. 16 — The phase by which the modulated scatterer speed leads the wave crest. Wave frequency = 0.575 Hz, U_0/C = 0.09; ♦ upwind look, ♢ downwind look.

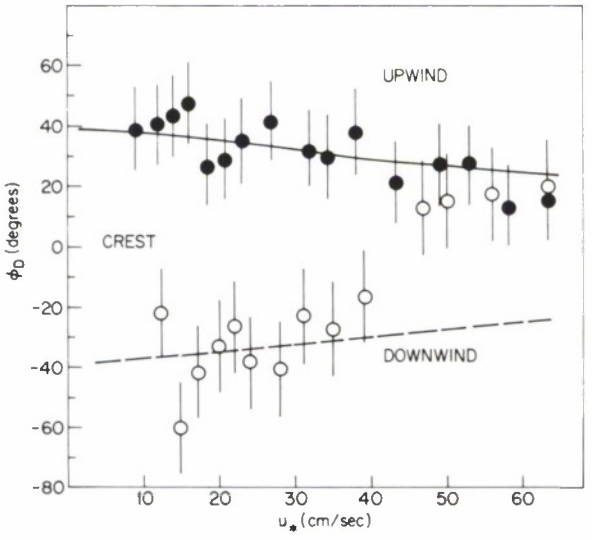

Fig. 17 — The phase by which the modulated scatterer speed leads the wave crest. Wave frequency = 1.1 Hz, U_0/C = 0.15; ♦ upwind look, ♢ downwind look.

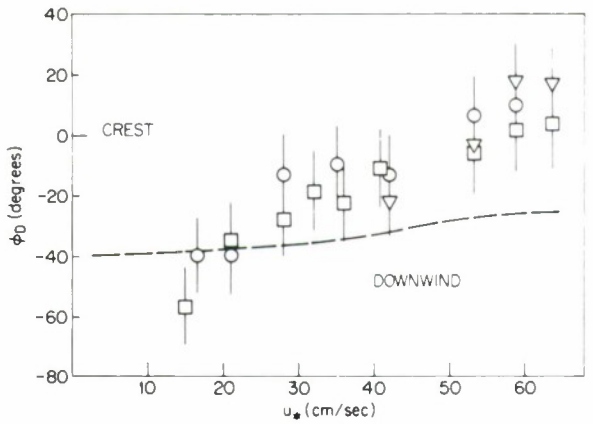

Fig. 18 — The phase by which the modulated scatterer speed leads the wave crest looking downwind. Wave frequency = 0.9 Hz, □ - amplitude = 7 cm, ▽ - amplitude = 6 cm, ○ - amplitude = 3 cm.

The first order (in U_0/C) terms in the expansion adequately describe the response of the wind-generated waves for winds of less than 7 to 8 m/s and $U_0/C < 0.1$. For these winds and larger wave amplitudes, the fractional modulations saturated, i.e., they ceased to increase with increasing modulating wave amplitude. A likely cause is the diminution and/or redistribution of the spectral energy density of the wind-generated wave system illustrated by the capacitance probe measurements given in the section on wind drift. Such effects occur at second order in the expansion, Eq. (13). Though complicated and of practical importance, they do not necessarily represent a basic failure of the relaxation time model.

A related manifestation of higher-order straining is the dependence of the mean scattering cross-section on modulating wave amplitude. This is shown for three different winds in Fig. 19. The variation of cross section with amplitude is substantial at the intermediate wind but small or insignificant at the lowest and highest wind. This last slight variation is a little surprising in view of the virtually 100% modulation of scattered power at the largest wave amplitudes shown in Fig. 10. The cross section is also dependent on modulating wave frequency (Fig. 20) because it is presumably a function of slope or strain rather than of wave amplitude. Again however, the variation is slight at the highest wind. It is clear from these results that radar cross sections of two-scale wind-generated wave systems do depend on the amplitude of the larger scale components as well as on the windspeed. In attempting to assess the implication of these results for scattering from the ocean, however, it must be remembered that gravity waves of the order of 1 m in wavelength as encountered in the wave tank, are thought to be relatively independent of fetch and wind under most oceanic conditions. Furthermore, the variations in cross section reported here may well be fetch dependent on a wave-tank scale, and this has not been investigated.

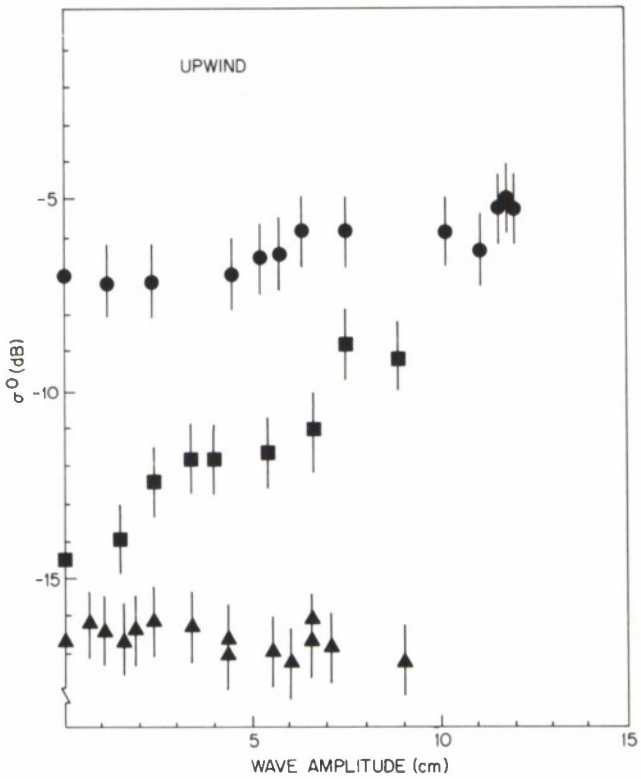

Fig. 19 — Scattering cross section looking upwind as a function of modulating wave amplitude. ● - u_* = 64 cm/s; 0.9 Hz, ■ - u_* = 30 cm/s, frequency = 0.575 Hz; ▲ - u_* = 16.5 cm/s, 0.575 Hz.

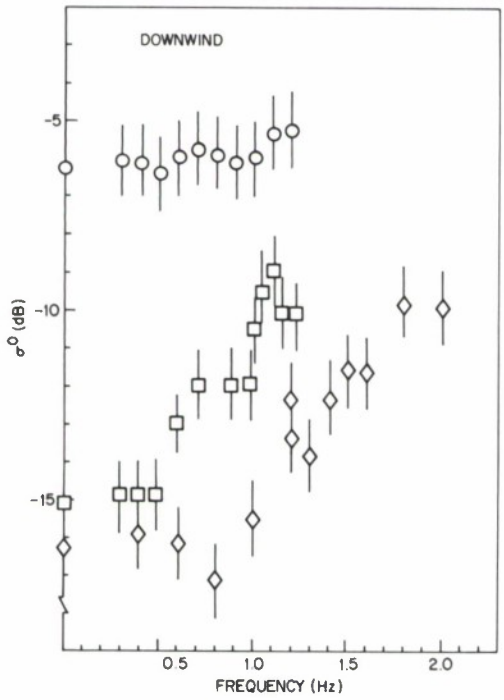

Fig. 20 — Scattering cross section looking downwind as a function of modulating wave frequency.

□ - u_* = 28 cm/s, A ≈ 5.5 cm
◇ - u_* = 28 cm/s, A = 1.2 - 2 cm (Fig. 15, bottom)
○ - u_* = 64 cm/s, A = 6.0 cm (Fig. 15, top)

Marked departure from the predictions of the relaxation time model, at air friction velocities greater than 40 cm/s, is shown by the coalescence of scatterers near or behind the wave crest at the higher winds (Figs. 8 and 9). That the scatterers are indeed the small wave system and not breaking water can be determined from the doppler spectra shown in Fig. 21. Breaking of the larger scale wave implies that the horizontal velocity of the breaking water equals or exceeds the phase speed. The doppler shift that results from a scatterer moving with horizontal velocity C is just C/λ_B, where λ_B is the Bragg wavelength; the position of this doppler shift is indicated in each of the three spectra in Fig. 21. Only in the case of the very large 0.9-Hz wave is there substantial scattering at this doppler shift. It is particularly noteworthy that this coalescence of scatterers occurs for moderate wave amplitudes (Fig. 8) for which $U_0/C = 0.09$ and the fractional modulation is only a few percent. This suggests that the departure from the model may occur at first order in U_0/C. The most puzzling feature of the results is the apparently oscillatory dependence of the phase ϕ_C of the modulated cross section upon the modulating wave frequency (Fig. 13). This behavior is essentially the same at two different modulating wave amplitudes and, with one or two exceptions, measurements from independent runs on different days agree within the estimated experimental error. Note that, as this error is essentially a linear boresighting error, the phase error in degrees is inversely proportional to modulating wavelength. There is a significant difference between the phase for 0.9-Hz waves measured at nominal fetches of 4 and 7 m.

Although the phase of the modulated line-of-sight scatterer speed depends significantly on the wind, the amplitude of this modulated speed, measured as described in this report, is equal to the line-of-sight orbital speed within 10% or 3 cm/s, whichever is greater. The influence of the augmented wind drift on the phase speed of the scatterers partially accounts for the windspeed dependence of the phase of the modulated speed. Downwind observations of phase (ϕ_D) of the modulated scatterer speed at 0.9 and 1.1 Hz and $u_* = 64$ cm/s, which show this speed to be in phase, or leading the crest, require unrealistically elongated elliptical scatterer orbits to explain them. Finally, the diminution of RMS wind-generated wave surface displacement by periodic gravity waves exhibits windspeed dependence opposite to that predicted by Phillips and Banner [10]. The neglect of direct coupling between wind and waves in the theory of Phillips and Banner is a likely reason for this failure of the theory.

OCEAN WAVE IMAGERY—A RECOMMENDATION

In a wind-wave tank, the amplitude of the gravity-wave modulation of microwave backscattering at 9.375 GHz and at a 45° depression angle strongly depends on the direction of microwave look with respect to the wind, as well as upon the windspeed and modulating wave amplitude. There are two identifiable modulating effects: the straining and tilting, respectively, of the wind-generated waves by the modulating gravity wave. In the case of modulation by a gravity wave of 1.75-s the tilting and straining effects are equal at a moderate wind where the straining has been substantially diminished by relaxation. The important parameter determining the relaxation behavior is the ratio of Bragg wave relaxation rate to modulating wave frequency. Large storm-aroused waves have periods of about an order of magnitude greater than the 1.75-s wave of the wave-tank experiments. If relaxation rates are proportional to Bragg wave number, a rough guess, the wave-tank measurements should

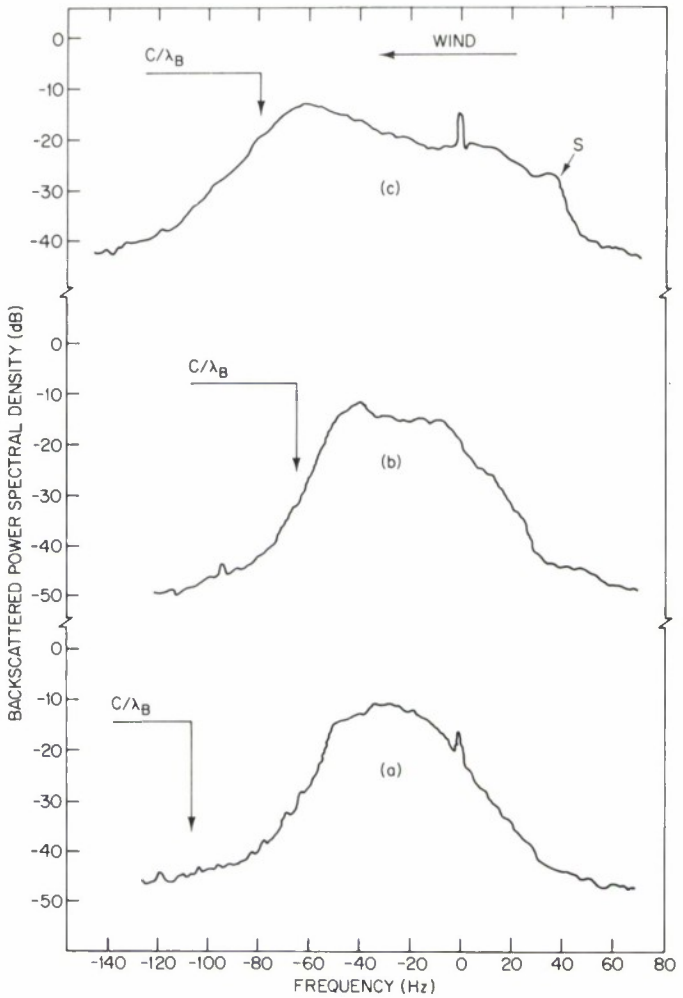

Fig. 21 — Doppler spectra looking upwind at $u_* = 64$ cm/s. (a) 0.575 Hz, C = 242 cm/s, $U_0/C = 0.09$; (b) 1.1 Hz, C = 145 cm/s, $U_0/C = 0.15$; (c) 0.9 Hz, C = 178 cm/s, $U_0/C = 0.36$.

approximately model L-band (1-GHz) scattering at sea. On a Bragg scattering model on vertical polarization, say, the first order modulation due to tilting is approximately proportional to $\tan\theta$, for $\theta > 45°$. The relative contributions of straining and tilting do not vary greatly over the range of depression angles envisaged for satellite-borne imaging radars. At lower depression angles and/or on horizontal polarization, the influence of tilting is relatively greater. However, 2-frequency X-band radar measurements [11] show that even at 15° the modulation is still very significantly dependent on windspeed. Consequently, wave image intensity due to amplitude modulation of the scattered microwave power is not a satisfactory measure of wave amplitude in most cases. By contrast, the modulated line-of-sight scatterer speed is directly related to wave amplitude; in the case of the long waves of the

ocean, which travel very rapidly compared to microwave Bragg wavespeeds, the influence of the wind is probably entirely negligible. If it is desired to obtain wave amplitudes from synthetic aperture radar signals, signal processing should emphasize the recovery of line-of-sight scatterer speeds or accelerations rather than treat them as phase errors in the imaging of stationary targets.

MOMENTUM TRANSFER

The phase of the amplitude-modulated backscatterer indicated that the small waves generally led the crest of the modulating waves at winds of less than 7 to 8 m/s. This would lead to momentum transfer to the larger wave if the modulated stress mechanism [12] outweighs the energy transfer mechanism of Hasselmann [2]. At higher winds, the small wave system lagged the crest, which could lead to large wave growth from either mechanism. However, the measured phase at higher winds exhibited a puzzling oscillatory dependence on modulating frequency and appeared to be fetch dependent. Further wave-tank modulation experiments are required before final conclusions can be drawn about momentum and energy transfer from short to long waves.

ACKNOWLEDGMENTS

The measurements reported here were made at the wave-tank facility of the University of Florida, Gainesville. The cooperation of O. Shemdin and the staff of that facility is gratefully acknowledged. These data were collected under contract NA 756-73 with the National Environmental Satellite Service.

REFERENCES

1. T.R. Larson and J.W. Wright, *J. Fluid Mech.* **70**, 417-436 (1975).

2. K. Hasselmann, *J. Fluid Mech.* **50**, 189-205 (1971).

3. W.C. Keller and J.W. Wright, *Rad. Sci.* **10**, 139-147 (1975).

4. T.R. Larson and J.W. Wright, "Wind-Wave Studies: Part 2 - The Parabolic Antenna as a Wave Probe," NRL Report 7850 (1974).

5. J.R. Duncan, W.C. Keller and J.W. Wright, *Rad. Sci.* 9, 809-819 (1974).

6. J.W. Wright and W.C. Keller, *Phys. Fluids* 14, 466-474 (1971).

7. O.H. Shemdin, *J. Phys. Oceanogr.* 2, 411-419 (1972).

8. W.C. Keller, T.R. Larson and J.W. Wright, *Rad. Sci.* 9, 1091-1100 (1974).

9. M.L. Banner and O.M. Phillips, *J. Fluid Mech.* 65, 647-657 (1974).

10. O.M. Phillips and M.L. Banner, *J. Fluid Mech.* 66, 625-640 (1974).

11. W.J. Plant, "Studies of Backscattered Sea Return with a Dual Frequency X-Band Radar," USNC/URSI Meeting, Urbana, Ill., June 1975.

12. J. Witting and J.W. Wright, *Report of NRL Progress*, 1-16, Feb. 1975.